MecSol2013
International Symposium on Solid Mechanics
April 18-19, 2013
Porto Alegre, Rio Grande do Sul, Brazil

Aeroelastic analysis of a delta wing considering geometric nonlinear behavior

Felipe Schaedler de Almeida
Graduate Program in Civil Engineering
Federal University of Rio Grande do Sul
felipe.almeida@ufrgs.br

Armando Miguel Awruch
Graduate Program in Civil Engineering
Federal University of Rio Grande do Sul
amawruch@ufrgs.br

ABSTRACT

Application of a partitioned procedure for the aeroelastic analysis of a delta wing immersed in a compressible flow is presented in this work. Structural and flow simulations are performed with different codes using the Finite Element Method (FEM). Geometrically nonlinear effects are incorporated to a triangular shell element with a corotational formulation. Compressible flow simulations are performed by the two-step explicit Taylor-Galerkin (T-G) method employing moving meshes based on the Arbitrary Lagrangian-Eulerian (ALE) formulation of the governing equations. Simple and efficient algorithms are adopted to deal with the information exchanged between non-matching meshes in the fluid-structure interface boundary and for the fluid mesh movement. The aeroelastic behavior of a steel delta wing due to flows with different dynamic pressures is investigated. Results compare very well with other numerical works, but good agreement with respect to experimental data is only obtained for tests with moderated wing displacements.

Keywords: Finite elements, Nonlinear dynamics, Aeroelasticity

1 INTRODUCTION

Determination of the interaction of fluid flow and flexible structures is a fundamental requirement in a growing number of engineering applications. Aeroelasticity is one of the most important classes of fluid-structure interaction (FSI) problems. It is particularly relevant for aeronautical designs, where structure is subjected to usually high speed air flow. This problem is characterized by a cyclic process where structure is deformed under aerodynamic forces and flow is modified due to change of solid boundary caused by structural displacements. The aeroelastic analysis is concerned with the significant mutual interaction among inertial, elastic and aerodynamic forces present in those cases [1]. The importance of these interaction phenomenon increases as more light and slender structures are obtained by the use of advanced materials and modern design techniques, adopted to achieve project requirements.

The objective of a FSI analysis is to determine the behavior of fluid-structure coupled system subjected to perturbations of the initial configuration. Depending on flow conditions these perturbations may be damped or they may grow indefinitely, producing a potentially catastrophic phenomenon

known as flutter. Alternatively, structural vibration may be sustained with limited amplitude. This phenomenon is known as limit cycle oscillation (LCO) and it is associated to the presence of nonlinearity in fluid and structure [2].

This work deals specifically with the aeroelastic analysis of a cropped delta wing, formed by a steel plate, in a compressible flow, which is a good representation of flexible wings of modern unmanned combat aircrafts [3]. The problem analyzed here was experimentally investigated by [4] for flow conditions with fixed Mach number but with dynamic pressures varying form values where LCO starts and growing until flutter takes place. Progressively more sophisticated approaches were used in the works of [5], [3], [2] and [6] for the numerical simulation of this problem. The increment of model complexity used for the FSI analysis enhanced simulation quality for cases with low amplitude LCO. However, numerical tests underpredicted wing vibrations for flow conditions close to flutter.

The present work investigates the application of a proposed numerical scheme to the aeroelastic analysis of the cropped delta wing studied by [4] and compare the results to previous numerical works on the same problem. The computational methods used for FSI analysis are presented in Section 2. The improved serial staggered scheme (ISS) [7] is adopted to solve the coupled problem, allowing to use independent methods for the simulation of fluid and structure. Information is transferred in fluid-structure boundary interface by the node-projection scheme [8], which showed to be efficient for the problem solved.

The explicit two-step Taylor-Galerkin scheme is employed for the simulation of compressible flows using tetrahedral finite elements for fluid domain discretization. An algebraic scheme is adopted to define the fluid mesh motion for adaptation to moving boundary determined by structure displacements. This method is very simple and numerical efficient, but there is no prevention with respect to excessive mesh distortion.

Structure is simulated using a triangular flat shell element [9] which is able to handle thin and moderately thick sections of isotropic or laminated composite materials. Geometrical nonlinearity is incorporated by the element independent corotational formulation (EICR) [10]. The nonlinear structural dynamic integration is performed by the implicit scheme called approximately energy-conserving corotational procedure (AECCP) [11].

2 COMPUTATIONAL METHOD

Theoretical aspects of computational methods adopted for solving FSI are briefly presented in the following sections. Structural analysis and fluid dynamic simulation are independently discussed due to partitioned nature of the FSI technique employed here.

2.1 Geometrically nonlinear structural dynamics

The finite element code implemented by [9] is adopted for the structural dynamic analysis. Spatial discretization is performed by 3-noded triangular shell elements with three translations and three rotations as nodal degrees of freedom. The shell element is formed by a membrane element formulated by [12] and a plate element developed by [13]. Moderately thick shell of isotropic materials or laminated composites can be considered and transverse shear deformation is taken into account by the first order theory (FSDT).

Geometrically nonlinear behavior is incorporated in the analysis by applying the element independent corotational formulation (EICR) [10] to the shell element, which is originally obtained from linear formulations. The main characteristic of EICR is the complete separation of corotational filtering of the deformational displacements from the core element formulation. Arbitrary large rotations and translations are correctly analyzed, but only small strain are allowed due to limitations of EICR

and core element formulation.

For each element, variations of deformational displacements $\delta\bar{\mathbf{p}}_d$ in the attached corotational system are obtained from variations of global displacements $\delta\mathbf{d}$ using the relation

$$\delta\bar{\mathbf{p}}_d = \bar{\mathbf{H}}\bar{\mathbf{P}}\,\mathbf{T}\delta\mathbf{d} = \mathbf{\Lambda}\,\delta\mathbf{d} \tag{1}$$

where the matrix $\mathbf{\Lambda} = \bar{\mathbf{H}}\bar{\mathbf{P}}\mathbf{T}$ comprises three operations, namely: local to global reference system transformation given by matrix $\mathbf{T}$, deformational displacements extraction by the projector matrix $\bar{\mathbf{P}}$ and conversion of spin vectors (representing variation of rotations in $\delta\mathbf{d}$) into additive rotations (used in $\delta\bar{\mathbf{p}}_d$ for compatibility with local element formulation), which is performed by the matrix $\bar{\mathbf{H}}$ and necessary when large rotations are present. Detailed discussions on corotational theory are given in references [14, 11, 15].

Time integration is performed using the approximately energy-conserving corotational procedure (AECCP). This implicit scheme was developed by [11] as an approximation to the corotational mid-point dynamic algorithm [16], and it was introduced in order to conserve the full energy of the mechanical system. It is a class of mid-point algorithm which is constructed by equating the change of total momentum of the body to the impulse of internal and external forces acting on the system during the time step [17]. The equilibrium equation is given by Eq.(2), where, $\Delta\phi^k$, $\Delta\phi^e$ and $\Delta\phi^i$ are the kinetic, external and strain energy increments in the time step, respectively.

$$\Delta\phi^k + \Delta\phi^i + \Delta\phi^e = (\mathbf{f}^T_{mas,m} + \mathbf{f}^T_{i,m} - \mathbf{f}^T_{e,m})\Delta\mathbf{d} = \mathbf{g}^T_m\Delta\mathbf{d} = 0 \tag{2}$$

$\mathbf{f}_{mas,m}$, $\mathbf{f}_{e,m}$ and $\mathbf{f}_{i,m}$ are the mid-point inertial, external and internal nodal element forces, respectively. The mid-point vectors form an equivalent force vector $\mathbf{g}_m$ that may vanish, approximately conserving the total energy of the system. In each time step the advance is conducted by a predictor step followed by corrector iteractions in order to approach $\mathbf{g}_m$ to zero, as described in [11] and [9]. The mid-point equilibrium condition adopted in AECCP is particularly suitable for the application in fluid-structure analysis with the partitioned scheme used in this work, which is described in Section 2.3. Previous experience in using AECCP for FSI analysis was reported by [18].

2.2 Computational fluid dynamics

In this work the unsteady compressible flow is modeled by the Euler equations, which are given in vectorial form by

$$\frac{\partial \boldsymbol{U}}{\partial t} + \frac{\partial \boldsymbol{F}_i}{\partial x_i} = \mathbf{0}, \quad (i = 1, 2, 3) \tag{3}$$

where $\boldsymbol{U}$ is the vector of conservation variables and $\boldsymbol{F}_i$ is the vector of advective fluxes in the x_i coordinate direction. A previous work [3] showed that Euler equations are well suited to this problem because viscous effects have low influence in the aeroelastic behavior of the cropped delta wing . For FSI analysis, flow equations must be integrated in a moving domain, which is accomplished by adopting the Arbitrary Lagrangian-Eulerian (ALE) description [19]. Based on ALE formulation Eq. (3) turns to

$$\frac{\partial \boldsymbol{U}}{\partial t} = -\frac{\partial \boldsymbol{H}_i}{\partial x_i} - \frac{\partial w_i}{\partial x_i}\boldsymbol{U}, \quad (i = 1, 2, 3) \tag{4}$$

with $\boldsymbol{H}_i = (\boldsymbol{F}_i - w_i\boldsymbol{U})$ and w_i being the velocity of the reference domain in the direction of coordinate x_i.

The explicit two-step Taylor-Galerkin method [20] is adopted for the nonlinear fluid solution. This scheme results from discretizing time dimension by a Taylor series expansion of $\boldsymbol{U}$ followed by the spatial discretizations of the resulting system of partial differential equations using the FEM. The Taylor series expansion of $\boldsymbol{U}$, which is assumed to be known at time n, results in

$$\Delta \boldsymbol{U} = \Delta t \frac{\partial \boldsymbol{U}^{n+1/2}}{\partial t} \tag{5}$$

where $\Delta \boldsymbol{U} = \boldsymbol{U}^{n+1} - \boldsymbol{U}^{n}$ and

$$\frac{\partial \boldsymbol{U}^{n+1/2}}{\partial t} = -\frac{\partial \boldsymbol{H}_i^{n+1/2}}{\partial x_i} - \frac{\partial w_i}{\partial x_i}\boldsymbol{U}^{n+1/2} \tag{6}$$

with $\boldsymbol{U}^{n+1/2} = \boldsymbol{U}^{n} + 0.5\Delta t \frac{\partial \boldsymbol{U}^{n}}{\partial t}$.

The system of conservation equations given in Eq. (5)–(6) is decoupled, so that the spatial discretization using FEM can be applied to each equation separately, and it may be written in a general form as

$$\Delta u = \Delta t \left(-\frac{\partial h_i^{n+1/2}}{\partial x_i} - \frac{\partial w_i}{\partial x_i} u^{n+1/2} \right) \tag{7}$$

Applying Galerkin method to Eq. (7), with u, h_i and w_i approximated by interpolation of nodal values ($\bar{\mathbf{u}}$, $\bar{\mathbf{h}}_i$ and $\bar{\mathbf{w}}_i$) using element shape functions $\mathbf{N}$ and interpolating $u^{n+1/2}$ by piecewise constant functions $\mathbf{P}_{(e)}$ gives, after integrating by parts,

$$\begin{aligned} &\int_{V_e} \mathbf{N}\mathbf{N}^T \, dV \, \Delta \bar{\mathbf{u}} = -\Delta t \int_{V_e} \frac{\partial \mathbf{N}}{\partial x_i} \left(h_i^{n+1/2} \right) dV \\ &- \Delta t \frac{\partial w_i}{\partial x_i} \int_{V_e} \mathbf{N}\mathbf{P}_{(e)} \, dV \hat{u}^{n+1/2} + \Delta t \int_{A_e} \mathbf{N} \left(h_i^{n+1/2} \right) n_i \, dA \end{aligned} \tag{8}$$

where n_i is the component of the normal vector in the boundary of the domain. $\hat{u}^{n+1/2}$ represents u evaluated in the center of the element in time $n + 1/2$, which is explicitly defined by Eq. (9) in terms of known variables at time n when linear tetrahedron elements are adopted for spatial discretization of the fluid domain

$$\hat{u}^{n+1/2} = \left(1 - \frac{\Delta t}{2} \frac{\partial w_i}{\partial x_i} \right) \hat{u}^{n} - \frac{\Delta t}{2} \frac{\partial \mathbf{N}^T}{\partial x_i} \bar{\mathbf{h}}_i^{n} \tag{9}$$

Using linear tetrahedron elements also simplifies the integration in Eq. (8), which becomes explicitly defined and it may be evaluated after solving Eq. (9) in the same loop over the elements [20, 21], improving the computational efficiency. The system of equations resulting from spatial and temporal discretization is solved iteratively using the following equation

$$\Delta \tilde{\mathbf{u}}_{i+1} = \tilde{\mathbf{M}}_L^{-1} \left(\tilde{\mathbf{r}} - \tilde{\mathbf{M}} \Delta \tilde{\mathbf{u}}_i \right) + \Delta \tilde{\mathbf{u}}_i \tag{10}$$

where $\tilde{\mathbf{M}}$ and $\tilde{\mathbf{M}}_L$ are the consistent and lumped mass matrices, respectively, $\tilde{\mathbf{r}}$ is the vector resulting form the integrals in the right hand side of Eq. (10) and the tilde indicates a global array. Artificial dissipation [22] is introduced in order to prevent oscillations of flow fields, which may occur in the proximity of shock regions due to numerical instabilities [23]. The size of the time steps is limited by Courant-Friedrichs-Lewy condition (CFL), as it is usual in explicit schemes.

In FEM analysis of FSI problems the mesh must move in order to accommodate the deflections of the flexible bodies that determine part of the boundary of the fluid domain. The mesh velocity field is independent with respect to fluid motion and must be defined by a separate formulation. In this work a very simple algebraic scheme is adopted for this purpose. The velocity of a given internal node i of the fluid mesh is determined by the velocity of the closest fluid node j lying in the moving boundary belonging to the structure. It is given by the following expression

$$\mathbf{w}_i = \left(\frac{a_{ij}}{a_{ij} + a_{ik}} \right) \mathbf{w}_j \tag{11}$$

where $a_{ij} = (d_{ij})^{-m}$ is a coefficient determined by the distance d_{ij} form the internal node i to a node j in the moving boundary while a_{ik} depends on the distance to the closest node in the fixed portion of the boundary. The exponent m determines the variation of influence of boundary velocity over the mesh velocity in the interior of the domain, being adopted as 3 in all problems solved in this work.

2.3 Fluid-structure interaction

The improved serial staggered (ISS) procedure due to [7] is employed to solve the nonlinear aeroelastic problem in the current work. This is a loosely coupled time integrator allowing fluid-structure analysis using specialized methodologies for each field. Compatibility and equilibrium conditions in the fluid-structure interface is achieved without subiterations. ISS is shown to be third-order accurate in terms of energy transfer [24] and coupling time steps comparable to monolithic methods and strongly coupled methods can be used, maintaining good solution accuracy [7].

The steps of the adopted staggered algorithm are schematically illustrated in Fig. 1. A time-lag equal to half of the coupling time step exist between fluid and structure integration, ensuring satisfaction of geometric conservation law [25]. Due to this characteristic, mid-point rule algorithms like AECCP are particularly suitable to use with ISS, since mid-point external load $f_{e,m}$, presented in Eq. (2), is directly obtained by fluid forces over the wet surface.

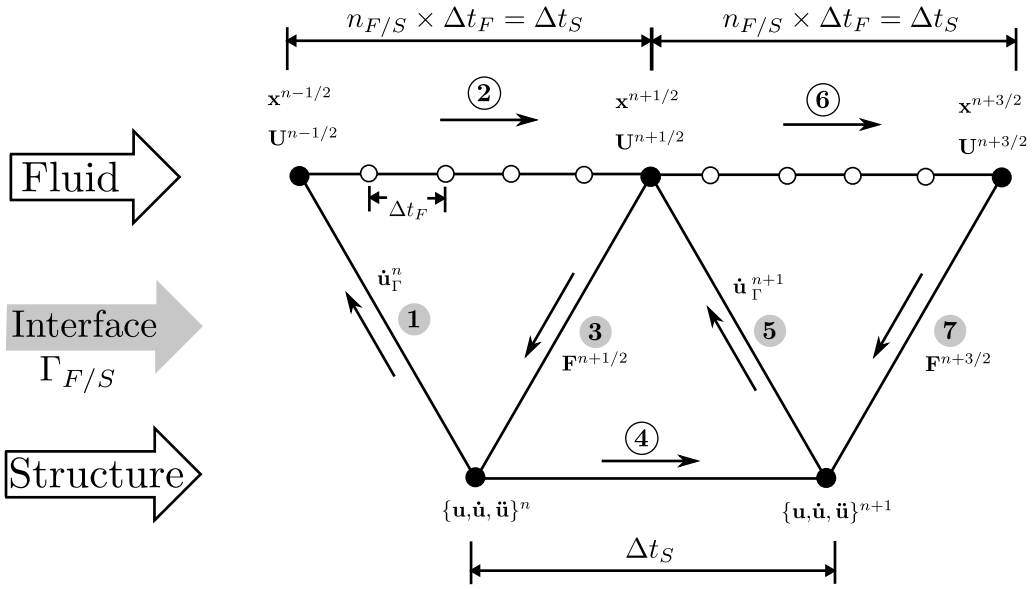

Figure 1: Improved Stagered Scheme with subcicling

Fluid-subcycling is adopted in order to efficiently accommodate the different time steps Δt_F and Δt_S required by the explicit CFD solver and the implicit structural dynamic solver, respectively.

A number of fluid time steps $n_{F/S} = \Delta t_S / \Delta t_F$ is performed for each coupling time step, which is taken equal to Δt_S.

Fluid and structure meshes are non-matching in their interface boundaries and they are handled in order to allow the most efficient discretization for each medium. Fluid forces $\mathbf{F}_F$ and structural velocity $\dot{\mathbf{u}}_E$ are transmitted between non-matching interfaces by the node-projection scheme [8], as depicted in Fig. 2. Each fluid node i on fluid-structure interface boundary $\Gamma_{F/S}$ is projected on a structural element e, and natural coordinates of point i into the element ($\boldsymbol{\zeta}_i$) are calculated.

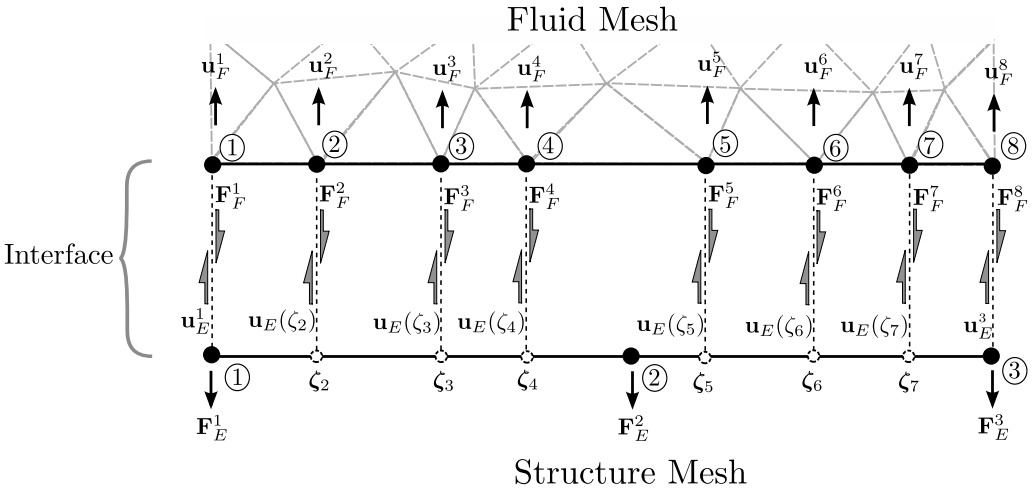

Figure 2: Nodal projection scheme

Fluid forces are transferred to a structural nodes j by

$$\mathbf{F}_E^j = \sum_{e=1}^{n_e} \left(\sum_{i=1}^{n_f} N_E^j(\boldsymbol{\zeta}_i) \mathbf{F}_F^i \right)_e \tag{12}$$

where n_f is the number of fluid nodes i projected on each one of the n_e structural elements connected to node j and N_E^j is the element shape function corresponding to this node. A similar procedure, given in Eq. (13), is employed to transfer velocity from the structural mesh to fluid nodes in $\Gamma_{F/S}$.

$$\dot{\mathbf{u}}_F^i = \sum_{j=1}^{nnel} N_E^j(\boldsymbol{\zeta}_i) \dot{\mathbf{u}}_E^j \tag{13}$$

3 NUMERICAL TESTS

This section reports the application of the computational methods described above to FSI analysis of a crooped delta wing, which planform is shown in Fig. 3. The structure is formed by a 0.888 mm thick plate of steel with blunt trailing and leading edges and clamped boundary condition at the root. Material properties are: Young's modulus of 200 GPa, Poisson's ratio of 0.3 and specific mass of 7850 kg/m^3.

Figure 4 presents the 20×20 structured FEM mesh employed for the structure discretization in all tests.

The natural mode shape and frequencies of the wing are calculated using the FEM mesh of Fig. 4. Results obtained are shown in Fig. 5 and agree very well with data reported by other authors [4, 2, 6], ensuring FEM model validity.

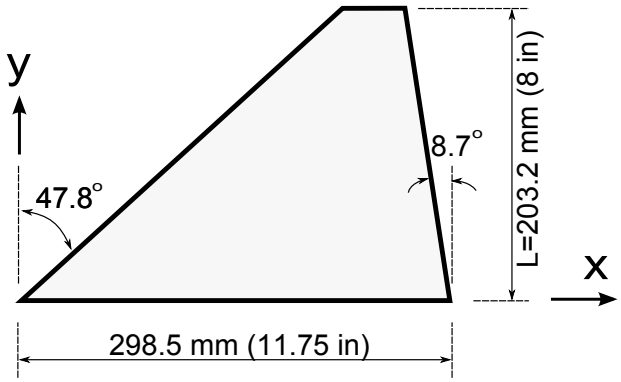

Figure 3: Wing geometry

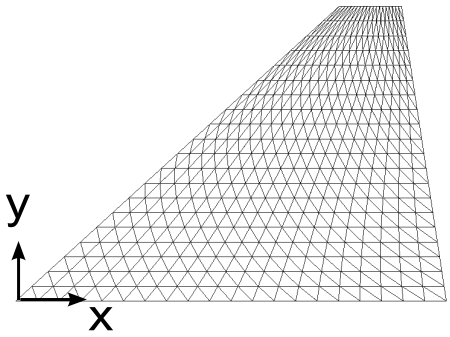

Figure 4: Mesh for the cropped delta wing

Wind-tunnel flow conditions reported by [4] are used for the simulations in the current work. A Mach number equal to 0.87 and zero angle of attack are fixed. Dynamic pressures[1] of 2.58 psi ($17.79kPa$) and 2.98 psi ($20.55kPa$) are adopted for the investigation of the wing aeroelastic behavior.

An unstructured FEM mesh with more than 2.5 million tetrahedrons and 445 thousand nodes is employed for the fluid discretization. About 32 thousand nodes are on the fluid-structure boundary interface. Figure 6 shows the FEM mesh over the wing and some details close to the leading edge and the tip of the wing, where more refined discretization is necessary. Initial flow conditions are obtained by a previous converged steady state simulation over an undeformed wing configuration. The fluid-structure interaction is triggered by a perturbation of the structure in the form of a initial velocity field proportional to its first bending mode.

The aeroelastic behavior of the wing has been experimentally investigated by [4] and many numerical works [3, 2, 6] have been conducted trying to simulate the observed phenomena. The analyses performed in this work are presented together with comparison to available references.

The flow conditions used for FSI analyses correspond to the beginning of the dynamic pressure rage investigated in [4] experiments and previous computational works related to this problem [2, 6]. A Courant number of 0.2 is adopted for the CFD algorithm and $\Delta t_e = 5.0 \times 10^{-5} s$ is used for the structural time-marching scheme.

Figure 7 depicts the dynamic response of the wing by the dimensionless displacement of the

[1]Pressure is given in psi (1 psi = 6895Pa) in order to easy comparison with other authors

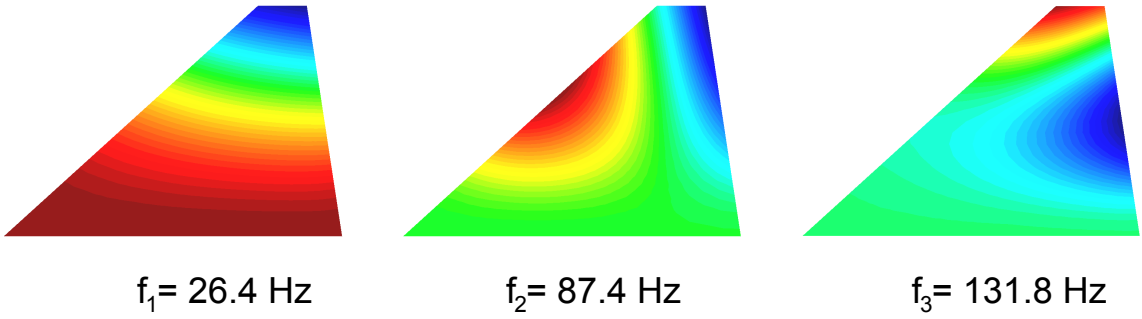

Figure 5: Natural frequencies and mode shapes of the wing

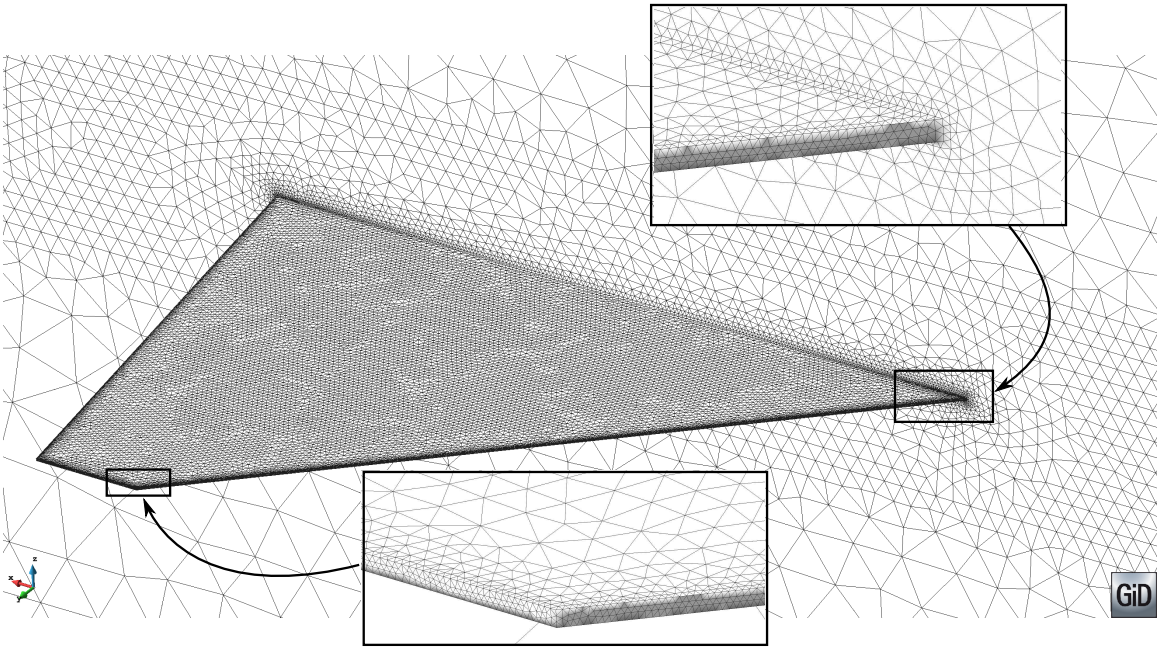

Figure 6: Mesh of the fluid close to the cropped delta wing

trailing-edge tip, when subjected to a dynamic pressure equal to 2.58 psi. The limit-cycle oscillation (LCO) phenomenon is observed after a brief transient motion. Maximum amplitude $u_z/L = 0.028$ and oscillation frequency $f = 43.5Hz$ obtained in this work are compatible with experimental measurements [4] $u_z/L \cong 0.030$ and $f \cong 43.6Hz$.

Simulation with a dynamic pressure of 2.98 psi resulted in a wing behavior similar to that of the previous analysis, as it is shown in Fig. 8, where LCO amplitude $u_z/L = 0.062$ and frequency $f = 45.5Hz$ are observed. Results of current work are almost the same of those obtained by [6], which are the best numerical simulation reported for this case, but LCO amplitude is significantly lower than the experimental value ($u_z/L = 0.1$).

Previous studies [3, 2, 6] reported increasing discrepancies between computer simulations and experimental results for flows with higher dynamic pressures. The apparent cause of this behavior is the inability of employed CFD models to reproduce all important aerodynamic phenomena when the wing develops large displacements. Results of reference [6] corroborate this assumption since incorporation of advanced structure models considering material and geometrical nonlinearities together with enhanced schemes for load and displacements transfer in fluid-structure interface boundary were

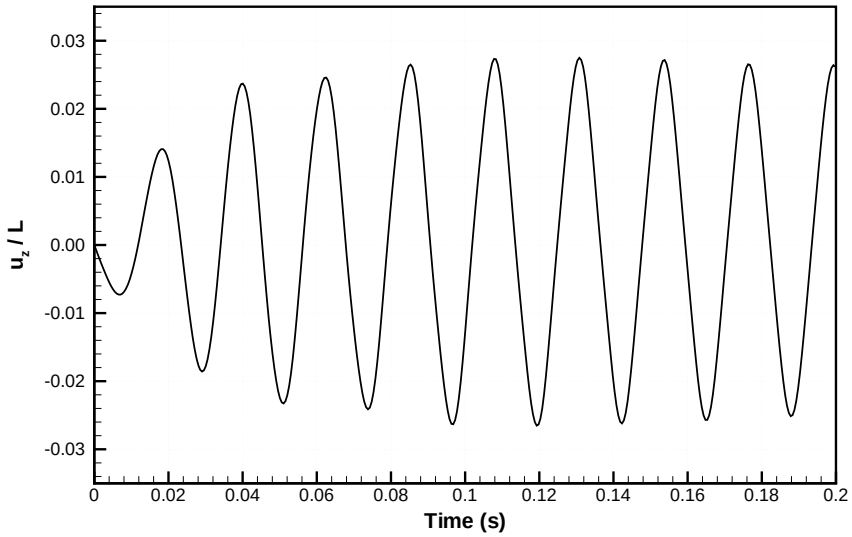

Figure 7: Wing tip displacement for q = 2.58 psi

not able to significantly improve the FSI analysis.

Figure 9 shows the pressure field of the flow over the wing deformed configuration (with $\times 10$ magnification) at time t = 0.1625s. A low pressure region occurs at the leading-edge, where the onset of aerodynamic effects may occur. However, these aerodynamic effects can not be reproduced by the mesh or the inviscid flow model employed in this study.

Time history of drag force (Fr_x), lift force (Fr_z) and moments about x and y axes are presented in figures 10, 11 and 12, respectively. These aerodynamic effects are calculated in the fluid mesh over the fluid-structure boundary (designated *flu*) and in the mesh of the structure (designated *str*). Transmission of aerodynamic forces from the fluid to the structure at the interface is demonstrated to be correct by the perfect match of the quantities measured using data of each mesh over the entire simulation.

It is observed from figures 8 and 11 that lift is 180 degrees out of phase with respect to wing transverse displacement, acting as a springlike force that always restores the wing to its undeformed configuration. The same condition is reported by [4], where lift was considered to be proportional to the angle of attack that was actually measured in the experiment. This phenomena is assumed to be the mechanism responsible for sustaining LCO since no net gain or loss of energy occurs during each cycle.

The history of the number of fluid subcycles for each structure time step ($n_{F/E}$) during FSI analysis with a dynamic pressure of 2.98 psi is shown in Fig. 13. A periodic variation similar to wing vibration is observed, demonstrating that fluid critical time step is dependent of flow condition and mesh distortion. The mean value of $n_{F/E}$ is 2090 and 2103 for simulations with dynamic pressures of 2.58 psi and 2.98 psi, respectively.

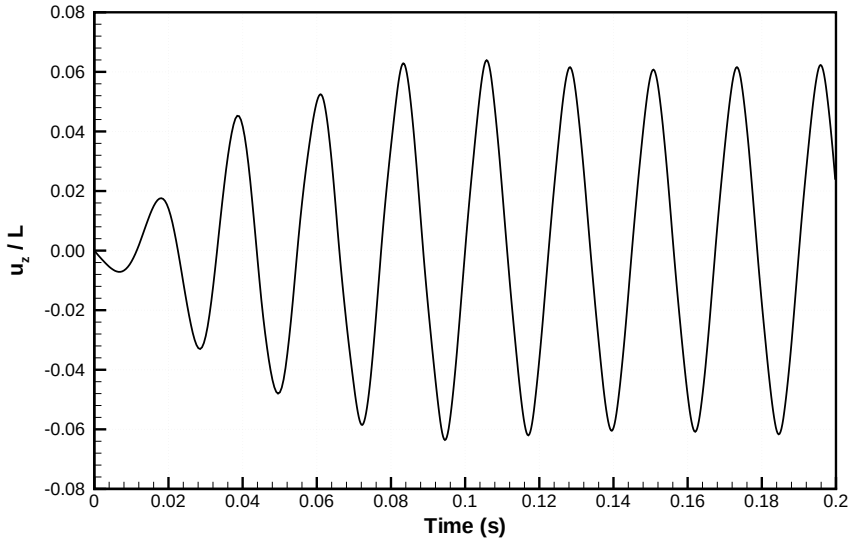

Figure 8: Wing tip displacement for q = 2.98 psi

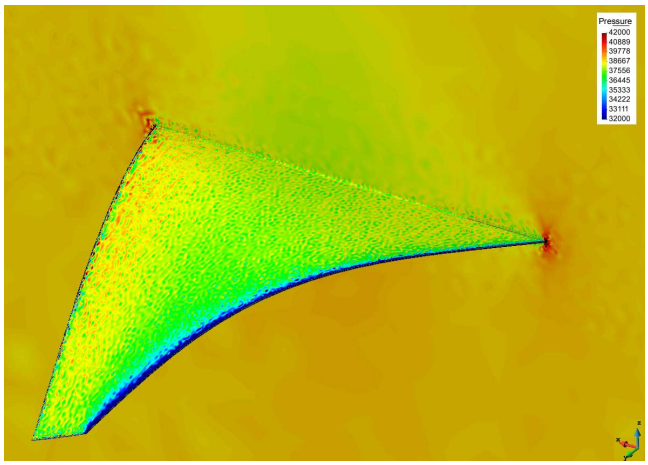

Figure 9: Pressure over the wing for q = 2.98 psi

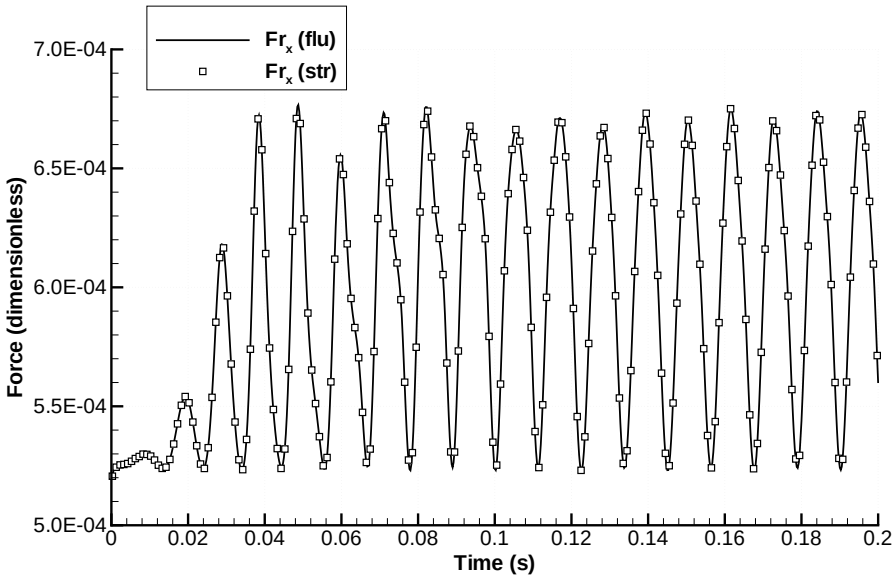

Figure 10: Drag (Fr_x) due to aerodynamic forces for q = 2.98 psi

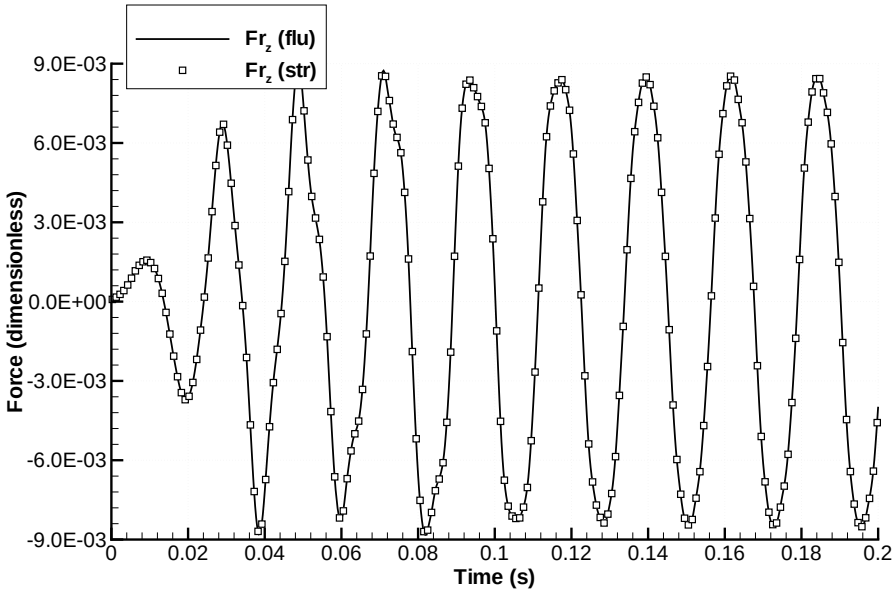

Figure 11: Lift (Fr_z) due to aerodynamic forces for q = 2.98 psi

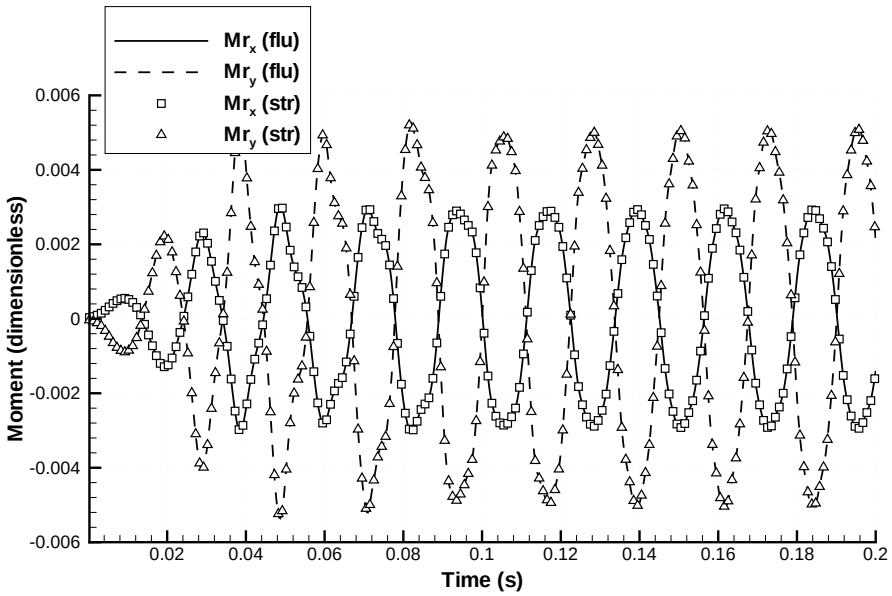

Figure 12: Moment due to aerodynamic forces for q = 2.98 psi

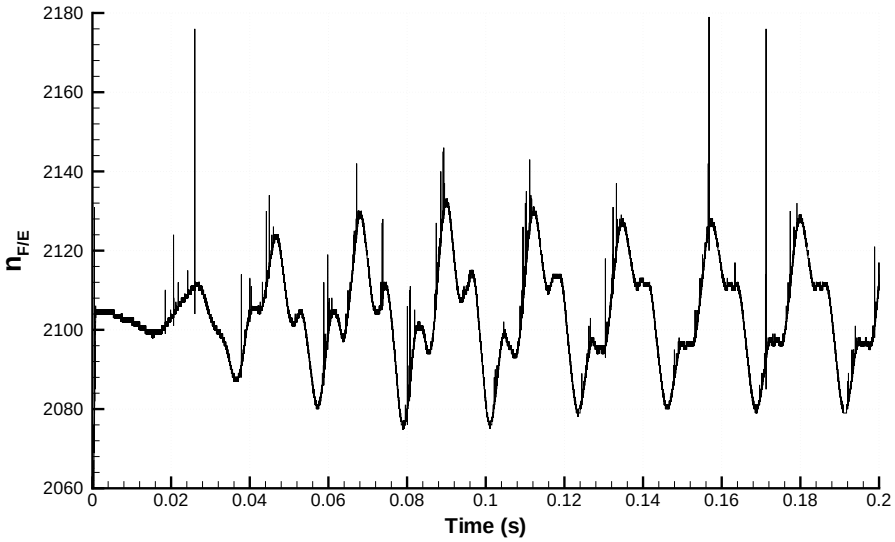

Figure 13: Fluid subcycling $n_{F/E}$ for q = 2.98 psi

4 CONCLUSIONS

In spite of simple algorithms used in this work for mesh movement and load transfer in the FSI boundary interface, the results presented here are very close to the best numerical simulations reported by other authors for the same problem. The methodology was best suited for cases where wing displacements have moderate amplitudes, resulting in small instantaneous local angles of attack during simulation. The identification of flow conditions when a wing perturbation is damped by the fluid or when LCO phenomenon takes place can be performed under limitations mentioned above.

It is also shown that correct FSI simulations can be obtained when shell elements are used to model the structure. The inherent gap between FSI interfaces due to the structural modeling in this case is pointed by [6] to be one of the reasons of poor results obtained in past works due to the reduced accuracy in load transfer. Simulations confirmed that lift and wing displacements are 180 degrees out of phase as supposed by [4], who related the oscillatory behavior to this condition.

5 AKNOWLEDGEMENTS

The authors wish to thank the Brazilian agencies CNPq and CAPES for their financial support. Authors are also very thankful to National Center for Super-Computing at Federal University of Rio Grande do Sul CESUP/UFRGS for providing the computational infrastructure.

REFERENCES

[1] R. Clark, D. Cox, H.C.J. Curtiss, J.W. Edwards, K.C. Hall, D.A. Peters, R. Scanlan, E. Simiu, F. Sisto, T.W. Strganac, et al. *A Modern Course in Aeroelasticity*. Solid Mechanics and Its Applications. Springer, 2004.

[2] P.J. Attar and R.E. Gordnier. Aeroelastic prediction of the limit cycle oscillations of a cropped delta wing. *Journal of Fluids and Structures*, 22(1):45 – 58, 2006.

[3] Raymond E. Gordnier. Computation of limit-cycle oscillations of a delta wing. *Journal of Aircraft*, 40(6):1206–1208, 2003.

[4] Edward T. Schairer and Lawrence A. Hand. Measurements of unsteady aeroelastic model deformation by stereo photogrammetry. *Journal of Aircraft*, 36(6):1033–1040, 1999.

[5] Raymond Gordnier and Reid Melville. Numerical Simulation of Limit-cycle Oscillations of a Cropped Delta Wing Using the Full Navier-Stokes Equations. *International Journal of Computational Fluid Dynamics*, 14:211–224, 2001.

[6] Jinglong Han Cui Peng. Numerical investigation of the effects of structural geometric and material nonlinearities on limit-cycle oscillation of a cropped delta wing. *Journal of Fluids and Structures*, 27(4):611 – 622, 2011.

[7] M. Lesoinne and C. Farhat. Higher-Order Subiteration-Free Staggered Algorithm for Nonlinear Transient Aeroelastic Problems. *AIAA Journal*, 36:1754–1757, September 1998.

[8] C. Farhat, M. Lesoinne, and P. Le Tallec. Load and motion transfer algorithms for fluid/structure interaction problems with non-matching discrete interfaces: Momentum and energy conservation, optimal discretization and application to aeroelasticity. *Computer Methods in Applied Mechanics and Engineering*, 157(1-2):95 – 114, 1998.

[9] F.S. Almeida and A.M. Awruch. Corotational nonlinear dynamic analysis of laminated composite shells. *Finite Elements in Analysis and Design*, 47(10):1131 – 1145, 2011.

[10] C. C. Rankin and F. A. Brogan. An element independent corotational procedure for the treatment of large rotations. *Journal of Pressure Vessel Technology*, 108(2):165–174, 1986.

[11] M. A. Crisfield. *Non-linear Finite Element Analysis of Solid and Structures - Vol2: Advanced Topics*. Wiley, 1997.

[12] Carlos A. Felippa. A study of optimal membrane triangles with drilling freedoms. *Computer Methods in Applied Mechanics and Engineering*, 192(16-18):2125 – 2168, 2003.

[13] Y.X. Zhang and K.S. Kim. A simple displacement-based 3-node triangular element for linear and geometrically nonlinear analysis of laminated composite plates. *Computer Methods in Applied Mechanics and Engineering*, 194(45-47):4607 – 4632, 2005.

[14] C.A. Felippa and B. Haugen. A unified formulation of small-strain corotational finite elements: I. theory. *Computer Methods in Applied Mechanics and Engineering*, Vol.194(21-24):2285 – 2335, 2005.

[15] B. Nour-Omid and C. C. Rankin. Finite rotation analysis and consistent linearization using projectors. *Computer Methods in Applied Mechanics and Engineering*, Vol.93(3):353 – 384, 1991.

[16] M.A. Crisfield and J. Shi. Co-rotational element/time-integration strategy for non-linear dynamics. *International Journal for Numerical Methods in Engineering*, Vol.37(11):1897 – 1913, 1994.

[17] M.A. Crisfield, U. Galvanetto, and G. Jelenic. Dynamics of 3-d co-rotational beams. *Computational Mechanics*, Vol.20(6):507 – 519, 1997.

[18] A. Relvas and A. Suleman. Fluid-structure interaction modelling of nonlinear aeroelastic structures using the finite element corotational theory. *Journal of Fluids and Structures*, 22(1):59 – 75, 2006.

[19] Thomas J.R. Hughes, Wing Kam Liu, and Thomas K. Zimmermann. Lagrangian-eulerian finite element formulation for incompressible viscous flows. *Computer Methods in Applied Mechanics and Engineering*, 29(3):329 – 349, 1981.

[20] O.C. Zienkiewicz, R.L. Taylor, and P. Nithiarasu. *The Finite Element Method For Fluid Dynamics*. The Finite Element Method. Elsevier Butterworth-Heinemann, 2005.

[21] P.R. Lohner. *Applied Computational Fluid Dynamics Techniques: An Introduction Based on Finite Element Methods*. John Wiley & Sons, 2001.

[22] P. Nithiarasu, O.C. Zienkiewicz, Satya Sai, B.V.K., K. Morgan, R. Codina, and M. VÃązquez. Shock capturing viscosities for the general fluid mechanics algorithm. *International Journal for Numerical Methods in Fluids*, 28(9):1325–1353, 1998.

[23] J. Argyris, I.St. Doltsinis, and H. Friz. Studies on computational reentry aerodynamics. *Computer Methods in Applied Mechanics and Engineering*, 81(3):257–289, 1990.

[24] Serge Piperno and Charbel Farhat. Partitioned procedures for the transient solution of coupled aeroelastic problems - part ii: energy transfer analysis and three-dimensional applications. *Computer Methods in Applied Mechanics and Engineering*, 190(24-25):3147 – 3170, 2001.

[25] C. Farhat and M. Lesoinne. Two efficient staggered algorithms for the serial and parallel solution of three-dimensional nonlinear transient aeroelastic problems. *Computer Methods in Applied Mechanics and Engineering*, 182(3-4):499 – 515, 2000.